REPORT DOCUMENTATION PAGE

Form Approved
OMB No. 0704-0188

AD-A265 179

2. REPORT DATE	3. REPORT TYPE AND DATES COVERED
05-20-93	Technical 06-01-92 to 05-31-93

4. TITLE AND SUBTITLE
Absorption Spectrum Calculations Using Mixed Quantum-Gaussin-Wave Packet Dynamics

5. FUNDING NUMBERS
N00014-90-J-1209

6. AUTHOR(S)
K. Haug and H. Metiu

DTIC
ELECTE
MAY 28 1993
S C D

7. PERFORMING ORGANIZATION NAME(S) AND ADDRESS(ES)
University of California
Department of Chemistry
Santa Barbara, CA 93106

8. PERFORMING ORGANIZATION REPORT NUMBER
T7

9. SPONSORING/MONITORING AGENCY NAME(S) AND ADDRESS(ES)
Office of Naval Research
Chemistry Program
800 N. Quincy Street
Alexandria, VA 22217

10. SPONSORING/MONITORING AGENCY REPORT NUMBER

11. SUPPLEMENTARY NOTES
Prepared for Publication in J. Chem. Phys. (submitted)

12a. DISTRIBUTION/AVAILABILITY STATEMENT
Approved for public release;
distribution unlimited

93-11989

13. ABSTRACT (Maximum 200 words)

We calculate the absorption spectrum of a cluster using a computational method in which classical-like degrees of freedom for the nuclei are described by Gaussian wave packets while the valence electrons are treated quantum mechanically. We examine the spectral features in comparison to an even simpler mixed quantum-classical model in which the nuclear motion is treated by purely classical mechanics. Anomalous features (such as negative absorption) in the absorption spectrum which can arise from mixed quantum-classical methods are examined and the Gaussian wave packet nuclear dynamics is found to substantially reduce these anomalous features. This method is applied to a two-coordinate model problem in which exact numerical results can be obtained and we find that the method works fairly well. We also apply the method to the valence electronic absorption spectrum for a KXe_6 cluster. The method does not suffer from the dramatic failure seen when Xe motion is treated classically. The method is used to calculate the vibrational width and the vibrational structure of the electronic absorption spectrum.

14. SUBJECT TERMS	15. NUMBER OF PAGES
	45
	16. PRICE CODE

17. SECURITY CLASSIFICATION OF REPORT	18. SECURITY CLASSIFICATION OF THIS PAGE	19. SECURITY CLASSIFICATION OF ABSTRACT	20. LIMITATION OF ABSTRACT
Unclassified	Unclassified	Unclassified	UL

NSN 7540-01-280-5500

Standard Form 298 (Rev. 2-89)
Prescribed by ANSI Std. 239-18
298-102

Submitted: J. Chem Phys.

ABSORPTION SPECTRUM CALCULATIONS USING MIXED QUANTUM-GAUSSIAN WAVE PACKET DYNAMICS

Kenneth Haug

Department of Chemistry

Lehigh University

Bethlehem, PA 18015

and

Horia Metiu

Department of Chemistry and Physics

University of California

Santa Barbara, CA 93106

Abstract: We calculate the absorption spectrum of a cluster using a computational method in which classical-like degrees of freedom for the nuclei are described by Gaussian wave packets while the valence electrons are treated quantum mechanically. We examine the spectral features in comparison to an even simpler mixed quantum-classical model in which the nuclear motion is treated by purely classical mechanics. Anomalous features (such as negative absorption) in the absorption spectrum which can arise from mixed quantum-classical methods are examined and the Gaussian wave packet nuclear dynamics is found to substantially reduce these anomalous features. This method is applied to a two-coordinate model problem in which exact numerical results can be obtained and we find that the method works fairly well. We also apply the method to the valence electronic absorption spectrum for a KXe_6 cluster. The method does not suffer from the dramatic failure seen when Xe motion is treated classically. The method is used to calculate the vibrational width and the vibrational structure of the electronic absorption spectrum.

I. Introduction

There is an enormous literature concerning computational methods and applications in which some degrees of freedom are treated quantum mechanically and some are treated classically or semiclassically[1,21]. The basic idea is that light particles, such as electrons, require a quantum description while nuclei may or may not depending upon the specific application.

There is also a large literature concerning the errors made by treating some degrees of freedom classically and others quantum mechanically [13,16,22-28]. There is as yet no precise criterion that can be used to establish in advance when one is guaranteed to obtain accurate results, but the existing computational experience allows us to guess the likelihood of success. The outcome depends to a large extent on the quantity being computed. Calculations of the expectation value of an observable, given by an expression of the form , $\langle \Psi(t) | O | \Psi(t) \rangle$, where O is an operator and $| \Psi(t) \rangle$ is the time dependent wave function of the system are often successful. They do however tend to fail if the wave function for the quantum degrees of freedom consists of "pieces" localized in different regions of the space.[11,13,16,26] Quantities of the form $\langle \Psi(t) | O | \Psi(0) \rangle$ which appear in calculations of various rates (e.g. photon absorption and Raman scattering, radiationless transitions, etc.) are more difficult. Model calculations have shown, for example, that calculations of the absorption cross section lead to unacceptable results, such as fairly large negative absorption rates. The reason for this failure was determined[21] by numerical analysis using various levels of approximations, for a model for which exact numerical results were also obtained. In

conventional mixed quantum-classical (QC) calculations only the evolution of the quantum degrees of freedom is represented by a wave function. The time dependent positions of the particles treated classically appear parametrically in the Hamiltonian for the quantum degrees of freedom. The evolution of these classical degrees of freedom - obtained by solving an "effective" Newton equation - provides a time dependent force acting on the quantum degrees of freedom. For example, the quantum particle could be an electron and the classical particles, nuclei. If the nuclei oscillate at a certain frequency, the force they exert on the electron will oscillate at this frequency, and one may expect that this oscillating force will correctly generate the vibrational structure in the spectrum. The results[21] do not bear out this expectation. The reason is simple. In the quantum theory, the spectral information is contained in the time evolution of the overlap integrals between the initial nuclear wave function and the same wave function at time t. The QC theory does not provide a wave function for the nuclear wave functions and therefore this overlap is set equal to one. This error is compounded by the fact that the nuclei act on the electron with a time dependent force. If the nuclei were not allowed to move, setting the nuclear overlap to one will merely kill the vibrational bands in the spectrum; moving them classically brings about negative rates.

Metiu and Haug [21], who pointed out this unpleasant feature, suggested a model that will remedy the situation without adding much to the computational burden: to treat the nuclear motion by Heller's Gaussian Wave Packet (GWP) method.[29a] This is known to give good results in short time calculations and to fail for long times. Procedures that will give better long time results[29b] tend to

become computationally expensive, defeating the main reason for the GWP approximation. This impasse is resolved by an important observation made by Nitzan (private communication), in the context of the theory of radiationless transitions, which is also applicable to absorption rate calculations considered here. In our case we must calculate the evolution of the system in the "promoted state" [30] , $\mathbf{r}\,|\,\Psi(0)\rangle$, where **r** is the electron position and $|\,\Psi(0)\rangle$ is the ground state of the system. The nuclei, which started out at their equilibrium positions, corresponding to the state $|\,\Psi(0)\rangle$, are out of equilibrium with respect to the state $\mathbf{r}\,|\,\Psi(0)\rangle$. As a result, the nuclei will start to move as soon as the electron is "promoted" and the overlap integral of their current wave function with their initial wave function will start going down. If the electron interacts with N nuclear degrees of freedom, we will have a product of N overlap integrals, all becoming less than one. While each overlap may change little (i.e. from 1.0 to 0.8) the product will plummet rapidly. Thus for systems with many degrees of freedom we only need a short time calculation to determine the vibrational broadening of the spectrum. During this short time, the nuclei cannot sample much of the potential energy surface, which can then be represented by a local harmonic approximation. . Because of this a GWP calculation of the nuclear overlap should be very accurate.

In this article we explore numerically how this works for two cases. In both cases, there is a single valence electron treated quantum mechanically while the nuclei are treated by GWP - and we denote this combined method QGWP. The first case is a two-coordinate test model mimicking an alkali-helium dimer that we have previously used[21] for the examination of other QC methods. In this

case, because of the simplicity of the model, we can examine exact quantum mechanical and also exact quantum Hartree calculations as benchmarks for comparison with the QGWP method. The second case we examine is an application to a 3-dimensional cluster with realistic potentials mimicking KXe_6. In this cluster, the three dimensional motion of the valence electron is treated quantum mechanically while the nuclear motion is treated by the GWP approximation. The initial condition is the quantum mechanical ground state for the electron and the GWP approximation for the ground state of the nuclei. To calculate the absorption cross section, the electron is promoted and propagated by a Fast Fourier Transform (FFT) method[33] while the nuclear wave function evolves according to Heller's GWP method.

In Section II, we outline the theory behind these calculations. In Section III the two-coordinate test model is presented and in Section IV the KXe_6 cluster is examined.

II. THEORY

II.A. Introduction

We consider a cluster containing a single valence electron (located at **r**), the parent ion core with charge +1 and N "solvent" atoms (located at $\mathbf{R} = \{ \mathbf{R}_\alpha , \alpha=1,2,3...,N+1 \}$). The corresponding momenta are **p** and **P** respectively. The Hamiltonian is

$$H = H_a(\mathbf{R},\mathbf{P}) + H_e(\mathbf{r},\mathbf{p};\mathbf{R}). \qquad \text{(II.1)}$$

H_a , describing the atomic degrees of freedom (i.e. the motion of the ion core and the solvent atoms), is given by

$$H_a = \sum_{\alpha=1}^{N+1} \mathbf{P}_\alpha^{\,2} / (2M_\alpha) + V_a(\mathbf{R}) , \qquad \text{(II.2)}$$

where $V_a(\mathbf{R})$ is the sum of the ion-solvent and the solvent-solvent interaction energies.

H_e , describing the valence electron degrees of freedom, is given by

$$H_e = \mathbf{p}^2/(2m) + V_{ea}(\mathbf{r},\mathbf{R}) \qquad \text{(II.3)}$$

containing the kinetic energy of the electron plus the interaction energy, V_{ea} , which is a sum of the electron-ion and the electron-solvent interaction energies.

II.B. Absorption Spectrum

To calculate the absorption cross section $\sigma(\omega)$ for the cluster configuration Γ, we use a slight variation of Heller's formula[31]

$$\sigma(\omega) \sim \omega \, \mathrm{Re} \int_0^\infty dt \exp(i\omega t) \, C(t) . \qquad \text{(II.4)}$$

The overlap integral C(t) is given by

$$C(t) = \exp(iE_g t/\hbar) \langle \Psi_p(0) | \Psi_p(t) \rangle, \qquad \text{(II.5)}$$

where E_g is the total ground state energy of the system and where the promoted state at time zero, $| \Psi_p(0) \rangle$, is

$$| \Psi_p(0) \rangle = -e \, \varepsilon \cdot \mathbf{r} | \Psi_g(0) \rangle \qquad \text{(II.6)}$$

In Eq.(II.6) $| \Psi_g(0) \rangle$ is the electronic and nuclear ground state, $-e\mathbf{r}$ is the dipole operator and ε is the electric field polarization direction. The promoted state at time t is

$$| \Psi_p(t) \rangle = \exp(-iHt/\hbar) | \Psi_p(0) \rangle . \qquad \text{(II.7)}$$

This formulation provides the absorption spectrum to all the excited states (including the photo-emission spectrum) in one calculation. The computations needed to evaluate Eq.(II.5) are made possible by using pseudopotentials to

describe the electron-ion and electron-solvent interactions resulting in an one electron problem, and by approximating the nuclear dynamics in some manner.

II.C. A summary of the time dependent Hartree approximation

In all QC methods the division of the degrees of freedom into classical and quantum ones is made by using a Hartree product wave function approximation. For calculating the spectrum, we use a Hartree product for the promoted state wave function [see Eq.(II.5)]

$$\langle \mathbf{r},\mathbf{R} | \Psi_p \rangle \approx \langle \mathbf{r} | -e\mathbf{r} | \phi_g \rangle \langle \mathbf{R} | \chi_g \rangle \exp(i\eta/\hbar) = \langle \mathbf{r} | \phi_p \rangle \langle \mathbf{R} | \chi_g \rangle \exp(i\eta/\hbar). \qquad (II.8)$$

Since our interest here is in electric dipole spectroscopy, the dipole operator is $-e\mathbf{r}$, and therefore only the ground state electronic wave function, $|\phi_g\rangle$, is "promoted" to, $|\phi_p\rangle$, while the ground state nuclear wavefunction, $|\chi_g\rangle$, is unaffected. In Eq. (II.8), as is typical in time-dependent Hartree (tdH) approximations, a time dependent phase term, $\exp(i\eta(t)/\hbar)$, is separated out to simplify the form of the tdH equations as[32]

$$i\hbar \frac{\partial}{\partial t} |\phi_p\rangle = [\, \mathbf{p}^2/2m + \langle \chi_g | V_{ea}(\mathbf{r},\mathbf{R}) | \chi_g \rangle / \langle \chi_g | \chi_g \rangle \,] \, |\phi_p\rangle, \qquad (II.9)$$

$$i\hbar \frac{\partial}{\partial t} |\chi_g\rangle = [\, \mathbf{P}^2/2M + V_a(\mathbf{R}) + \langle \phi_p | V_{ea}(\mathbf{r},\mathbf{R}) | \phi_p \rangle / \langle \phi_p | \phi_p \rangle \,] \, |\chi_g\rangle. \qquad (II.10)$$

and

$$\frac{\partial}{\partial t} \eta_g = \langle \phi_p \chi_g | V_{ea}(\mathbf{r},\mathbf{R}) | \chi_g \phi_p \rangle / \langle \chi_g | \chi_g \rangle \langle \phi_p | \phi_p \rangle \qquad (II.11)$$

The Hartree product wave function for the promoted state applied to the correlation function of Eq.(II.5) leads to a "Hartree" correlation function

$$C_h(t) = \exp(iE_g t/\hbar)\,\langle\phi_p(0)\,|\,\phi_p(t)\rangle\,\langle\chi_g(0)\,|\,\chi_g(t)\rangle\,\exp(i[\eta_g(t)-\eta_g(0)]/\hbar)\,, \tag{II.12}$$

with a Hartree ground state energy given by

$$E_g = \langle\phi_g\,|\,\mathbf{p}^2/2m\,|\,\phi_g\rangle / \langle\phi_g\,|\,\phi_g\rangle + \langle\chi_g\,|\,\mathbf{P}^2/2M+V_a(\mathbf{R})\,|\,\chi_g\rangle / \langle\chi_g\,|\,\chi_g\rangle +$$
$$\langle\phi_g\chi_g\,|\,V_{ea}(\mathbf{r},\mathbf{R})\,|\,\chi_g\phi_g\rangle / \langle\chi_g\,|\,\chi_g\rangle\,\langle\phi_g\,|\,\phi_g\rangle\,. \tag{II.13}$$

We note that due to the broken correlation in the Hartree product state, that the effective potentials (the averages over V_{ea}) in Eq.(II.9-11) become time dependent and can give rise to time varying energy levels in the system. This variation of the energy levels in time can result in serious problems in the absorption spectrum: unphysical negative amplitudes can appear as examined in Ref. 21 . Therefore any method that begins with the Hartree separation, such as the one we use here, will be susceptible to this problem. A failure to include the amplitude and phase information arising from the classical-like degrees of freedom will tend to magnify, possibly to a catastrophic extent (Ref. 21), the spectroscopic anomalies that can arise even at the Hartree level. Our quest is to minimize these anomalous effects by building an approximate, easy to evaluate wave function. By using the GWP method we can generate the quantum amplitude and phase information associated with the classical-like nuclear degrees of freedom, which is needed for the absorption cross section calculation.

II.D The QGWP method

The wave function , $\chi_g(\mathbf{R},t)$, representing the "classical-like" nuclear degrees of freedom, $\mathbf{R}$, and the integrals involving χ_g will be approximated because of the computational complications arising from the many dimensional character of χ_g. If we examine the Hartree equation (II.10) for $\chi_g(\mathbf{R},t)$ we see that the effective Hamiltonian for these "classical-like" degrees of freedom is

$$H_{eff} = \mathbf{P}^2/2M + V_{eff} \tag{II.14}$$

$$V_{eff} = V_a(\mathbf{R}) + \langle\phi_p | V_{ea}(\mathbf{r},\mathbf{R}) | \phi_p\rangle / \langle\phi_p | \phi_p\rangle . \tag{II.15}$$

Moving to the classical limit we take Eq.(II.14) as the effective classical Hamiltonian for the atoms in the cluster. Classical trajectories for the effective classical Hamiltonian in terms of the Cartesian coordinates and momenta are given by

$$\frac{d}{dt} P_\alpha = - \frac{d}{dR_\alpha} V_{eff}(\mathbf{R}) , \tag{II.16}$$

$$\frac{d}{dt} R_\alpha = P_\alpha / M_\alpha . \tag{II.17}$$

In the QC dynamic mixture we also make approximations for the integrals occurring in Eq.(II.9, 11 and 13) over the $\mathbf{R}$ coordinates of the forms:

$$\langle\chi_g | V_{ea}(\mathbf{r},\mathbf{R}) | \chi_g\rangle / \langle\chi_g | \chi_g\rangle \sim V_{ea}(\mathbf{r}, \langle\mathbf{R}\rangle) , \tag{II.18a}$$

$$\langle\phi_g\chi_p | V_{ea}(\mathbf{r},\mathbf{R}) | \chi_g\phi_p\rangle / \langle\chi_g | \chi_g\rangle \langle\phi_p | \phi_p\rangle \sim \langle\phi_p | V_{ea}(\mathbf{r}, \langle\mathbf{R}\rangle) | \phi_p\rangle / \langle\phi_p | \phi_p\rangle , \tag{II.18b}$$

$$\langle\phi_g\chi_g | V_{ea}(\mathbf{r},\mathbf{R}) | \chi_g\phi_g\rangle / \langle\chi_g | \chi_g\rangle \langle\phi_g | \phi_g\rangle \sim \langle\phi_g | V_{ea}(\mathbf{r}, \langle\mathbf{R}\rangle) | \phi_g\rangle / \langle\phi_g | o_g\rangle , \tag{II.18c}$$

$$\langle\chi_g | \mathbf{P}^2/2M + V_a(\mathbf{R}) | \chi_g\rangle / \langle\chi_g | \chi_g\rangle \sim \langle\mathbf{P}^2\rangle/2M + V_a(\langle\mathbf{R}\rangle) , \tag{II.18d}$$

where in the classical limit

$$\langle\mathbf{R}\rangle = \langle\chi_g | \mathbf{R} | \chi_g\rangle / \langle\chi_g | \chi_g\rangle \sim \mathbf{R}(t) . \tag{II.19a}$$

$$\langle\mathbf{P}^2\rangle = \langle\chi_g | \mathbf{P}^2 | \chi_g\rangle / \langle\chi_g | \chi_g\rangle \sim \mathbf{P}(t)^2 . \tag{II.19b}$$

are represented by the classical trajectories for $\mathbf{R}(t)$ and $\mathbf{P}(t)$.

The initial condition of the cluster, for a specified cluster size, is determined by finding a configuration of (possibly local) minimum energy. To be consistent with the classical equations, the minimum energy atomic configuration for the cluster is determined with respect to the effective classical potential V_{eff} by following its gradient with respect to a parameter τ

$$\frac{d}{d\tau}\mathbf{R} = -\nabla V_{eff}(\mathbf{R}) . \qquad (II.20)$$

Fluctuations are introduced in the early phase of the minimization algorithm so as to avoid the likelihood of falling into a local basin of the effective potential. The fluctuations are introduced by Monte Carlo (MC) sampling from the distribution

$$\exp\{-\beta V_a(\mathbf{R})\}\exp\{-\beta \langle \phi_g | V_{ea}(\mathbf{r},\mathbf{R}) | \phi_g \rangle\} , \qquad (II.21)$$

in which β gradually evolves from a high temperature (typically 1000K for the applications below) to a low temperature (typically 100K), as various configurations are generated by the MC procedure. Each sampling provides the ion core and the solvent atom positions $\mathbf{R}_I$, $\{\mathbf{R}_\alpha\}_{\alpha=1,..N}$ corresponding to a highly probable configuration. Because the electron excitation gap is much larger than k_BT , the electron is in the ground state and the matrix element appearing in Eq. (II.21) is equal to the ground state interaction energy of the electron for the given nuclear configuration. After this "cooling down" period we follow the gradient to the minimum effective potential configuration. The net effect of choosing the initial configuration in this way is that if the quantum-classical dynamic scheme is initiated without promoting the electron then nothing happens: the electron remains in the ground state and the cluster remains frozen in its configuration, which is the required behavior.

As a further computational convenience, we make an electronic Born-Oppenheimer approximation by ignoring the parametric $\mathbf{R}$ dependence of $\phi_p(\mathbf{r},t;\mathbf{R})$

when evaluating the gradient in Eq.(II.16 and 20); i.e. we drop the term involving $\frac{\partial}{\partial \mathbf{R}}\phi_p(\mathbf{r},t;\mathbf{R})$. We note that this parametric $\mathbf{R}$ dependence of $\phi_p(\mathbf{r},t;\mathbf{R})$ is included in the MC sampling of Eq(II.21) and if we established an initial configuration solely by the use of the MC sampling function (damped gradually to 0 K), a slightly different configuration would result than that given by the gradient method.

From the local minimum configuration, the initial condition for the GWP approximation for $\chi_g(\mathbf{R},t)$ is determined via a normal mode analysis about this stable configuration. The function $\chi_g(\mathbf{R},t)$ is then given by

$$\chi_g(\mathbf{R},t) = \prod_n g_n(t) \qquad \text{(II.22)}$$

where n runs over the 3N-6 vibrational modes of the N-atom cluster. Q_n and ω_n are The mass scaled normal mode coordinates, Q_n , and normal mode frequencies , ω_n , satisfying

$$\ddot{Q}_n + \omega_n^2 Q_n = 0 , \qquad \text{(II.23)}$$

are used to specify the initial normal mode wave functions

$$g_n(q,t=0) = (\omega_n/\pi\hbar)^{1/4} \exp[- \omega_n\{ q - Q_n(0) \}^2 / 2\hbar] \qquad \text{(II.24)}$$

used as the initial ground state wave function for the n-th mode. Inserting Eq.(II.24) into Eq.(II.22) gives the initial nuclear wave function.

The time evolution of the $g_n(q,t)$ wave functions is performed by Heller's version of Gaussian Wave Packet (GWP) dynamics[29] resulting in

$$g_n(q,t) = (\omega_n/\pi\hbar)^{1/4} \exp\{ (i/\hbar)[(i\omega_n/2)\{ q - Q_n(t) \}^2 + \Pi_n(t) \{ q - Q_n(t) \} - \gamma_n(t)] \} . \qquad \text{(II.25)}$$

We have used the initial conditions, given by Eq.(II.24), to set $\Pi_n(0) = 0$, $\gamma_n(0) = 0$, and also to argue that the frequencies, ω_n , which serve as time-dependent width parameters within the general form of the GWP dynamics, should be time independent for the relatively short times involved in low resolution spectral calculations (this is the frozen Gaussian version of GWP dynamics[29]).

The variable Π is the mass scaled normal mode momenta , i.e.

$$\Pi_\alpha = \frac{d}{dt} Q_\alpha \tag{II.26}$$

and the Gaussian phase parameter is determined from

$$\frac{d}{dt} \gamma_\alpha = (1/2)\Pi_\alpha^2 - V_{eff}(Q_\alpha) - \hbar\omega_\alpha/2 \, . \tag{II.27}$$

In Eq.(II.27) we use the local harmonic approximation

$$V_{eff}(Q_\alpha) = (1/2)\, \omega_\alpha^2\, Q_\alpha^2 + V_{zero} \tag{II.28}$$

with

$$V_{zero} = V_a(\mathbf{R}) + \langle \phi_p | V_{ea}(\mathbf{r},\mathbf{R}) | \phi_p \rangle / \langle \phi_p | \phi_p \rangle \, . \tag{II.29}$$

being evaluated with $\phi_p(t=0)$ and $\mathbf{R}(t=0)$. We emphasize that because we need only the short time behavior of the nuclear overlap integral, the local harmonic approximation should work very well.

We can interpret the dynamics expressed in the promoted state correlation function by saying that the promotion of the electron from the ground to the promoted state provides the energy to set the cluster into motion. So both the electronic excitations and the vibrational structure of those excitations are included in the correlation function.

II.E The trajectory approximation

A first approximation often used for condensed phase correlation

functions involving a system with a localized quantum component surrounded by more classical-like degrees of freedom is to take a mean field approach with respect to the classical-like coordinates. This approach builds in the effect of the average perturbation of the surrounding, classical-like, medium on the local quantum system of interest.

A simple correction to this mean field correlation function, within the spirit of QC dynamics, is to run trajectories for the classically treated degrees of freedom which give rise to a time dependent potential for the quantum degrees of freedom. That is, $H_e(\mathbf{r},\mathbf{p};\mathbf{R})$ in Eq. (II.3) becomes time dependent due to the time dependence of the classical position, $\mathbf{R}(t)$, in the potential energy operator component of H_e. Only the quantum component of the Hartree correlation function of Eq.(II.12) is kept, giving

$$C_{QCT}(t) = \exp(iE_g t/\hbar)\,\langle \phi_p(0) \mid \phi_p(t)\rangle\,, \qquad \text{(II.30)}$$

which we call the quantum-classical trajectory approximation (QCT) for the spectral correlation function.

How to choose the classical trajectories in the general case of any QC mixed method is problematic. By comparing to the tdH theory, Eq.(II.9-11), one finds that averaging over a bundle of classical trajectories maintains the spirit of integrating over all $\mathbf{R}$ in the tdH equations.[24] This scheme is self-consistent and energy conserving if the classical trajectories respond to a mean force (averaged over the quantum wave function) as given by Eq.(II.16-19) above. For the set of initial conditions specified in the paragraphs following Eq.(II.19), the bundle of

trajectories collapses to a single trajectory that is uniquely determined by the set of forces impinging on the frozen cluster configuration due to the excitation of the electron. Because of this unique initial condition giving rise to an unambiguous mean trajectory approximation, it is convenient to compare the results of the QCT theory to the QGWP theory for the spectroscopy applications examined below.

We note that compared to the tdH correlation function in Eq.(III.12), the trajectory approximation correlation function in Eq.(II.30) lacks the factor $\langle \chi_g(0) | \chi_g(t) \rangle$ involving wave functions for the classical-like degrees of freedom (and it also lacks the Hartree phase term). The underlying assumption in the trajectory approximation is that the time dependent potential, arising due to $\mathbf{R}(t)$, and appearing in the quantum Hamiltonian will act to remedy this deficiency. In nearly rigid systems where the static mean field approximation is fairly good, this seems reasonable. However, in more supple systems where energy transfer between the quantum and classical degrees of freedom distorts the classical positions significantly, it is obvious from the form of the tdH correlation function in Eq. (III.12) that the overlap of $\langle \chi_g(0) | \chi_g(t) \rangle$ is indispensable in obtaining the correct spectrum. For example, if the system is floppy enough that $\langle \chi_g(0) | \chi_g(t) \rangle$ goes to zero at some time t, then the overall correlation function is zero and in general a time dependence in the quantum Hamiltonian will not be able to account for this.

II.F Time-energy resolution

Heller has pointed out[31] the useful connection between the resolution of the absorption spectrum and the length of time in which the promoted state

explores the potential energy surface. Engel, Schinke, Henning and Metiu[30] have discussed in detail the method that we use to obtain dynamic information by taking the high resolution spectrum and smearing it out to generate a sequence of low resolution spectra.

To generate this spectral resolution we replace Eq. (II.4) by

$$\sigma(\omega;\tau) \sim \omega \, \mathrm{Re} \int_0^\infty dt \, \exp(i\omega t) \, f_\tau(t) \, C(t). \tag{II.31}$$

The "window" function

$$f_\tau(t) = \exp[-(t / \tau)^2]. \tag{II.32}$$

cuts off the time evolution of the overlap integral for times substantially longer than τ. In the frequency domain, this window function smears out the spectrum and generates a low resolution version having the resolution on the order $\Delta\omega = 2\pi/\tau$. Thus, a spectrum taken with the resolution $\Delta\omega$ contains information about the motion of the promoted state for a time $\tau = 2\pi/\Delta\omega$.

The introduction of this resolution time is, of course, an arbitrary parameter from a dynamics perspective. One advantage of including a "classical wave function" is that vibrationally broadened line widths of electronic transitions can develop more naturally on a time scale determined by the dynamics of the problem. As the classical wave functions move away from their initial positions, the overlap of the classical-like term, $\langle \chi_g(0) \mid \chi_g(t) \rangle$, in Eq.(II.12) decays with time. If the configuration of the promoted system is such as to prevent further

recurrences of $\langle \chi_g(0) | \chi_g(t) \rangle$ in time then a broaden line will remain in the spectrum that will be independent of τ (for τ large). If the configuration of the promoted system is such as to allow for recurrences of $\langle \chi_g(0) | \chi_g(t) \rangle$ in time, then vibrational fine structure will appear as τ increases and the spectral lines will continue to narrow with increases in the resolution time τ.

III. TWO COORDINATE TEST CASE

We examine here the electric dipole absorption spectrum of a colinear alkali-helium dimer. Since this two-coordinate model problem can be solved numerically at both the full quantum mechanical level and the full quantum Hartree level, we can evaluate the accuracy of the QGWP method. Computational details for the two-coordinate test case are given in Appendix A.

III.1 The model

The model described in Ref. 21 is used here. We consider an electron (located at r), an ion with charge +1 (of infinite mass at the coordinate origin), and a helium mass atom (at R). The model consists of two body interactions among the three species.

For the alkali ion - electron interaction energy V_{ei}, we use

$$V_{ei}(r) = -e^2/r_c \quad \text{for} \quad r < r_c$$
$$= -e^2/r \quad \text{for} \quad r_c < r \qquad \text{(III.1)}$$

In Eq.(III.1) e is the electron charge and r_c is a cutoff parameter that will be specified below. The expression in Eq.(III.1) has been used to represent alkali atoms by Parinello and Rahman[34] , Selloni,Carnevali,Carr and Parinello[10] , and Haug and Metiu[17] in a variety of three-dimensional calculations.

The electron-helium interaction energy is that used by Coker, Berne and Thirumalai [35] (for electron-xenon) with a large distance cut off,

$$V_{eh}(X) = \sum_n (a/X^4)\,[\, b/(c+X^6) - 1\,] \qquad \text{(III.2)}$$

where

$$X = \min \{ |r-R| , R_c \}, \qquad \text{(III.3)}$$

$a = 26.86$ eV Å^4 , $b = 108.0$ Å^6 , $c = 83.29$Å^6. The cutoff distance $R_c = 0.5$Å is introduced to make the potential finite (and constant) at short distances. The total electron interaction energy of Eq.(II.3) is the sum of these two terms

$$V_{ea}(r,R) = V_{ei}(r) + V_{eh}(r,R) . \qquad \text{(III.4)}$$

The alkali ion - helium interaction energy, constituting $V_a(R)$ of Eq.(II.2), is taken to be harmonic with $\omega = 0.1$eV and which roughly approximates the realistic potassium ion - xenon interaction given by Budenholzer, Gislason and Jorgensen[36].

III.2 Absorption spectrum

In Figure 1, we present the fundamental transition of the electronic absorption spectrum for this model problem calculated with the quantum Hartree approximation, Fig.1a, and the QGWP method, Fig.1b. The quantum Hartree method is calculated using Eqs.(II.9-12) with quantum dynamics for both degrees of freedom. This Hartree method produces a spectrum in which the major peaks are essentially exact when compared to a full quantum calculation[21]. The fundamental electronic transition given in Fig. 1 shows the vibrational fine structure arising from the 0.1eV dimer vibration in the 3 split lines. Ref. 21 presents details regarding the small spurious bumps and dips which appear surrounding the major peaks which are related to the lack of quantum

correlations inherent in a Hartree product assumption. Since the QGWP approximation uses a Hartree product, we cannot expect it to do better than time dependent Hartree.

As seen in Fig. 1, the QGWP spectrum is a reasonable representation of the quantum Hartree spectrum. The fundamental electronic transition appears with vibrational fine structure at nearly the same frequencies and with relative amplitudes preserved as well. The width of the spectral lines in Fig.1 is determined by the cutoff time of Eq.(II.32) ; a choice of τ=100fs was used in this case. This result provides us with a measure of confidence in applying the QGWP method to more complex and realistic situations where a comparison to a more precise method is computationally out of hand.

IV. KXe_n CLUSTER

We now apply and compare the QCT and the QGWP methods to a more complex and physically realistic model. We want to examine how the the absorption spectrum of the K atom is modified by the interaction with the Xe atoms forming the cluster. This difficult physical problem can be examined satisfactorily if we work with an atom consisting of one valence electron interacting with a simple two body pseudopotential centered on the ion. The potential is spherically symmetric, energy independent, and local. It is further assumed that electron-solvent and the ion-solvent interactions are two body interactions. While some of these assumptions can be improved, we see no reason at this time to increase the complexity of the calculations by treating some of the interactions at a higher level of accuracy than others. Our purpose here is to examine the methodology. In Section IV.1 we give a brief summary of the potentials used. The computational details for this application are given in Appendix A.

IV.1 Interaction Potentials

For the ion - electron interaction energy, V_{ei}, we use Eq.(III.1) with r_c =2.21Å which results in the correct ionization potential for the K atom (4.34eV). We note that the spectrum will be distorted in the high frequency region corresponding to transitions to final states whose outer turning points are close to or exceed r_c. In spite of the simplicity of this psuedopotential, the low resolution absorption spectrum of an isolated K atom, calculated with this potential, is similar to the measured one (see Table I, to be discussed below).

The xenon - electron interaction energy is that used by Coker, Berne and

Thirumalai [35], with a large distance cutoff. The total electron interaction with the *N xenon (solvent) atoms* is

$$V_{es} = \sum_{n} (a/R_n^4) [\, b/(c+R_n^6) - 1 \,] \qquad \text{(IV.2)}$$

where

$$R_n = \min \{ X_n , R_c \}, \qquad \text{(IV.3)}$$

X_n is the distance between the electron and the n-th atom, a = 26.86 eV Å^4 , b = 108.0 Å^6 , and c = 83.29Å^6. The cutoff distance R_c is introduced to make the potential finite (and constant) at short distances. The magnitude of R_c determines the "transparency" of the xenon atoms to the electron and we set R_c = 0.5Å. The effect of varying R_c is examined in Ref. 17. This potential has a shallow attractive well of 0.48eV at 2.4 Å, which for a single Xe cannot bind the electron.

The total electron-atom potential used in Eq.(II.3) is the sum of these terms

$$V_{ea}(\mathbf{r},\mathbf{R}) = V_{ei} + V_{es} . \qquad \text{(IV.4)}$$

For the xenon-xenon interaction, we use a pairwise Lennard-Jones potential[35],

$$V_{ss} = (1/2) \sum_{n,m} 4\varepsilon [- (\sigma/R_{nm})^6 + (\sigma/R_{nm})^{12}], \qquad \text{(IV.5)}$$

with the parameters ε = 1.9733 x 10^{-2}eV and σ = 4.0551Å. R_{nm} is the distance between the n-th and m-th xenon atoms.

The potassium ion -xenon interaction energy is[36]

$$V_{is} = \sum_{n} C_9 / R_{in}^{9} - C_6 / R_{in}^{6} - C_4 / R_{in}^{4}, \qquad \text{(IV.6)}$$

where R_{in} is the distance between the n-th xenon atom and the potassium ion, $C_9 = 9.70 \times 10^{+3}$ eV $Å^9$, $C_6 = 1.4104 \times 10^{+2}$ eV $Å^6$ and $C_4 = 2.908 \times 10^{+1}$ eV $Å^4$. This potential has a weak attractive well of 0.15eV at a distance of 3.4Å.

The total inter-atomic interaction used in Eq.(II.2) is then

$$V_a(\mathbf{R}) = V_{is} + V_{ss} . \qquad \text{(IV.7)}$$

IV.2 The spectrum of the isolated potassium atom

The absorption spectrum of the isolated K atom is obtained by including in the Hamiltonian only the ion - electron interaction in Eq.(IV.4). The absorption spectrum is given in Fig. 2a. We have examined it to provide a reference for determining the spectral changes caused by the presence of the Xe atoms. The calculated energies, oscillator strengths and peak frequencies for the K atom using the computational parameters discussed in Section III are compared to measured values[37] in Table I. The frequency of the fundamental peak and the oscillator strength of the first three peaks in the calculated spectrum are close to the experimental values (see rows 1-2 of Table I for the oscillator strengths and the peak frequency in our model of K versus real K).

The first two peaks in the spectrum are rather similar to those measured for the K atom and our results concerning these peaks are relevant to experiments performed on the KXe_n system. The calculated electronic transitions are found at about 1.64, 3.08 and 3.49eV while experimentally[37] the transitions occur at 1.61, 2.67 and 3.80 eV. Errors in the higher energy peaks are expected since the absorption energies of these peaks are in the energy range where the computational grid is cut off.

IV.3 KXe_6 cluster

The KXe_6 cluster, for the potentials specified in Section III, has a ground state minimum energy configuration of octahedral symmetry with K at the center and the Xe atoms located 3.45Å from the K center. The electronic absorption spectrum of this cluster is calculated using three alternative dynamics

approximations. In the first case, the cluster is frozen in its ground state equilibrium configuration and the spectrum is calculated by letting the promoted wave function interact with the Xe atoms. In the second and third cases we allow the atoms to move in response to the excitation of the electron. where this motion is calculated by the QCT method and also by the QGWP method.

We place the six Xe atoms symmetrically along the x,y and z axis with the K atom at the origin. The spectra shown in Fig. 2 were calculated with an electric field polarization direction in the ⟨ 0,0,1 ⟩ direction (along one of the K-Xe axes) ; and the spectrum in Fig. 3 uses an electric field polarization direction in the ⟨ 1,1,1 ⟩ direction (between the K-Xe axes).

In Fig. 2b we present the spectrum using the frozen KXe_6 cluster. The spectral lines are shifted due to the interaction of the electron with the surrounding Xe atoms. A resolution time of τ=150fs is used for the spectral window function, in Eq.(II.32). This frozen cluster spectrum has a blue shift of about 0.33eV compared to the lone K atom spectrum. The electronic transitions are at about 1.97, 3.36 and 4.13eV. The relative intensities of the first few lines are changed only slightly by the presence of the Xe (see Table I, row 2 versus row 3).

In Fig. 2c we present the spectrum of the KXe_6 cluster using the more traditional quantum-classical trajectory method (QCT of Section II.E) in which the nuclear overlap is left out. A resolution time of τ=150fs is used for the spectral window function, Eq.(II.32) , for this case. The spectrum for the QCT method shows a dramatic anomaly on the red side of the fundamental transition which arises as the cluster relaxes, in response to the promotion of the electron. This anomaly begins to appear at a resolution time of about τ = 60fs and becomes more pronounced with increasing values of τ . For values of τ > 200fs, the anomaly

dominates the spectrum. We point out that this ringing anomaly is not an artifact caused by aliasing in the Fourier transforms, but is a real effect due to the incorrect feedback between the quantum and classical degrees of freedom.[21] The relative peak positions (at about 1.96, 3.36 and 4.13eV) and intensities of the lines in the QCT spectrum in Fig. 2c are both in agreement with the frozen cluster spectrum of Fig. 2b (see also Table I, rows 3 and 4).

In Fig. 2d, the spectrum of the KXe_6 cluster using the QGWP method is presented. In this cluster the motion of the classical wave function, in the QGWP approximation, provides an intrinsic decay for the correlation function and we do not need to use a window function. The line widths are "natural" in the sense that they represent the decay of the vibrational overlap, which takes place in about 150fs.

The GWP wave function ,in Eq.(II.25), separates various physical effects entering in the nuclear wave function. It contains an amplitude (which for simplicity we keep constant in width) ,and a phase given by the classical action along the trajectory traced by the center of the packet along with a factor exp[$i\mathbf{p}_t\bullet(\mathbf{r} - \mathbf{r}_t)/\hbar$] associated with the momentum distribution of the packet. The spectrum is practically unchanged if we remove the phase of the GWP wave function. The main contribution to the spectrum comes from the amplitude term, which causes a decay of the nuclear overlap entering in the cross section formula. In fact if we suppress the phase information of the classical wave function for this system and calculate a spectrum for comparison with the spectrum of Fig. 2d , we find marginally perceptible differences on the scale give in Fig. 2d.

From the comparison of Fig. 2c and 2d, it is clear that the QCT

approximation has greater trouble with negative cross section values than QGWP. Never-the-less small negative cross sections do occur in the QGWP spectrum. Since such small anomalies also occur in the exact Hartree calculations (see Fig. 1 above and Ref. 16 and 21), it is quite possible that the anomalies seen in Fig. 2d are due to the Hartree product assumption made in Eq.(II.8) and that no method using a Hartree product wave function would improve on this.

Two other points need to be made when the QCT and the QGWP methods are compared. The relative oscillator strength of the spectral lines given by the two methods are considerably different (see Table I). The relative strength of the 2p,3p,4p,... transitions in the series, is principally governed by the electronic time-correlation matrix element, $\langle\phi_p(0)|\phi_p(t)\rangle$ in Eq.(II.12), which does not vary between the two methods. However the Hartree phase term, involving $\eta(t)$ in Eq.(II.12), which is left out in the QCT method causes most of the intensity difference between the two methods. This can be seen from Table I by comparing line 5 (the QCT method) , with line 6 (QCT with the Hartree phase term added), and line 7 (the QGWP method) .

A second difference between the QCT and the QGWP methods is the energy shift in the spectrum. The QGWP electronic transitions are at about 1.39, 2.79 and 3.55eV which is a red shift of about 0.57eV (for the fundamental) with respect to the QCT method. This shift is readily traced to the phase information in the classical wave function and the Hartree phase terms. The QGWP spectrum is also red shifted by about 0.25eV compared to the spectrum of the isolated K atom. While we are not aware of spectral data for small K/Xe clusters, experimental

data for K defects in Xe matrices at 1.54°K [38c] suggests three different sites for K in Xe, each of which show triplet patterns. Two sites have centers (of the triplet) showing blue shifts of the fundamental K absorption line of about 0.05eV and 0.02eV while the third shows a red shift of about 0.01eV. Assuming that our simplified potentials are accurate, the shift difference that we find could be explained by noting that the Xe matrices do not have the flexibility of the KXe_6 cluster where the Xe atoms have considerable room to relax. Over the course of the 150fs decay time of the nuclear overlap of the Xe atoms,the Xe aligned with the electric field polarization (which are most strongly affected by the promoted electron) relax by about 0.085 Angstroms, while the Xe atoms perpendicular to the electric field direction relax by about 0.039 Angstroms. Such a large relaxation is less likely in a matrix and this difference may explain the difference in the spectral shift. The Xe atoms in this small cluster tend to accommodate the "needs" of the electron and are therefore displaced in a way that lowers the energy of the excited state.

As noted above, in the K/Xe matrix experiments[38b,c] the fundamental K line splits into a triplet separated by about (0.01-0.02)eV. The first excited state of the valence electron in the octahedral KXe_6 cluster is also three-fold degenerate. Due to the symmetry of the cluster and the polarization directions chosen, this triplet does not appear in Figs. 2 and 3. For example, in the case of the ⟨ 0,0,1 ⟩ polarization direction, although the octahedral symmetry is broken by a tetragonal elongation ($O_h \rightarrow D_{4h}$)[39] as the Xe atoms along the polarization direction back away from the K center when the electron is promoted, the 2-fold states of the doublet are still orthogonal to the polarization direction. In the case

of the ⟨ 1,1,1 ⟩ polarization direction, the degeneracy is not lifted. For arbitrary, polarization directions the splitting may appear depending on the magnitude and time scale of the configurational changes occurring in the cluster upon excitation (see Section II.F above).

The normal mode frequencies of the excited cluster range from 1.4×10^{-3} to 2.5×10^{-2} fs^{-1}, giving recurrence times in the range of 250 - 4500fs. While our main interest has been in short time calculations, we have also carried out a calculation meant to observe the appearance of vibrational structure in the electronic spectrum. In Fig. 3a , the spectrum of the KXe_6 cluster using the QGWP method is presented for a polarization direction chosen in the ⟨ 1,1,1 ⟩ direction which perturbs all six Xe atoms equally. For this polarization direction the anomalous features that appeared in the QCT spectrum in Fig. 2c are again minimal. Also appearing in this spectrum is the beginning of a vibrational structure, which is more apparent when attention is focused upon Fig. 3b in which the fundamental peak of Fig. 3a is blown-up. The vibrational structure is characterized by an energy spacing of about 0.00166eV (13.4 cm^{-1}) which implies a corresponding time periodicity of about 2500fs. All six Xe atoms are dynamically equivalent for this polarization direction and a representative Xe-K distance is displayed in Fig. 4a for 4000fs. The motion of the Xe atoms is driven by the energy flow from the quantum mechanical degrees of freedom (the excited electron) into the classical-like degrees of freedom. This energy flow is indicated in Fig.4b for 4000fs. The classical energy , denoted "C" in Fig. 4b, is

$$E_C = \sum_{n=1}^{N} \mathbf{P}_n^2/2M_n + V_a(\mathbf{R}) \qquad \text{(IV.8)}$$

and is measured along the left axis while the quantum energy, denoted "Q" in

Fig. 4b, is

$$E_Q = \langle \phi_p | p^2/2m + V_{ea}(r,\langle R \rangle) | \phi_p \rangle / \langle \phi_p | \phi_p \rangle \qquad \text{(IV.9)}$$

and is measured along the right axis of the figure. From both Fig. 4a and 4b a vibrational time cycle of about 2500fs is apparent. Note also that the vibrational mode is not just excited in this case, but rather that energy flows into the classical coordinates over the first 700fs and then drains out of these coordinates in the 1700-2400fs time span, after which it cycles back in again. This emphasizes the significant coupling of the electronic and vibrational degrees of freedom in this system.

We note that for the calculations in Fig. 4 the total energy of the system, quantum plus classical, is conserved to better than 0.7 percent over the 4000fs run time. Further computational details are given in Appendix A.

V. Summary

We have examined a computational method in which a set of classical-like degrees of freedom are described by Gaussian wave packets while the others are treated quantum mechanically. This method was applied to a two-coordinate model problem in which exact numerical results could be obtained and we found that the method works fairly well. We have also calculated the electronic absorption spectrum for a KXe_6 cluster in a frequency range where the valence electron of the K atom is excited. The method does not suffer from the dramatic failure (negative absorption cross section) seen when Xe motion is treated classically. Moreover, it generates a reasonable spectrum. The use of Gaussian wave packets (GWP) is justified by the observation that the overlap of the nuclear wave function is likely to decay very rapidly, requiring only a short time calculation, for which the GWP method is accurate. The decay time is shorter for systems with many degrees of freedom and the accuracy of the method increases as the system becomes more complete.

The most interesting applications that we foresee are for several quantum systems imbedded in a condensed medium or a large cluster. In such systems the width of the spectrum is due to the vibrations of the medium as well as inhomogeneous broadening. This method can calculate the vibrational width and the vibrational structure.

Appendix A: Computational details

The initial ground state wave functions for both the quantum and Hartree cases are calculated by acting with exp(-αH) on an arbitrary trial wave function with the appropriate symmetry. As the real number α becomes larger, the wave function converges towards the ground state of the Hamiltonian H. For propagation, we use a method proposed by Fleck, Morris and Feit[33]. The numerical procedure has been described by Hellsing, Nitzan and Metiu[40] and has been used by others in similar contexts[41].

The quantum time propagation is performed with the algorithm of Fleck, Morris and Feit[33], as discussed in Ref. 17. In the QC calculations, we propagate the electron wave function for one time step, calculate the mean potential, update the classical positions , update the classical coordinates in the quantum electron Hamiltonian, propagate the quantum wave function for another time step, etc.[17]

In the two-coordinate model for the quantum calculations , a time step of 0.01fs is used and a spatial grid having 64 points and a spacing of 0.6 Å in the r-coordinate and a spatial grid having 96 points with a spacing of 0.067Å in the R-coordinate. The results were checked for convergence with respect to grid spacing and grid size. The classical trajectories are generated by using the Verlet algorithm[42] with a time step of 0.01 fs.

In the KXe_6 model for the quantum coordinates, a time step of 0.01fs is used and a 3-D spatial grid having 36 points and a spacing of 0.7 Å in each direction. The classical trajectories are generated by using the Verlet algorithm with a time step of 0.05 fs. The results were checked for convergence with respect to grid spacing, grid size, and time step.

ACKNOWLEDGMENT

This work is supported by NSF CHE91-12926. Acknowledgment is also made to the donors of The Petroleum Research Fund, administered by the ACS, for partial support of this research and also to a grant from Lehigh University.

REFERENCES

[1] The number of articles applying such a technique is so large that we mention here only a few recent articles [2-21] which illustrate the procedure and/or which are specifically discussed in this article.

[2] J.T. Muckerman, I. Rusinek, R.E. Roberts and M. Alexander, J. Chem. Phys. 65, 2416 (1976).

[3] W.H. Miller, J. Chem. Phys. 68, 4431 (1978) .

[4] S.D. Augustin and H. Rabitz, J. Chem. Phys. 69, 4195 (1978).

[5] D.J. Diestler, J. Chem. Phys. 78, 2240 (1983).

[6] J. Olsen and D. Micha, Int. J. Quantum Chem. 22, 971 (1982).

[7] G.D. Billing, Chem. Phys. 70, 223 (1982).

[8] A.M. Roberts and A.E. DePristo, Surf. Sci. 134, 338 (1983).

[9] Carr and Parrinello, Phys. Rev. Lett. 55, 2473 (1985).

[10] A. Selloni, P. Carnevali, R. Car and M. Parrinello, Phys. Rev. Lett. **59**, 823 (1987).

[11] G. Wahnstrom, B. Carmeli and H. Metiu, J. Chem. Phys. 88, 2478 (1988)

[12] C.Z. Wang, C.T. Chan and K.M. Ho, Phys. Rev. B 39, 8586 (1989).

[13] R. Alimi, R. B. Gerber, A.D. Hammerich, R. Kosloff and M. A. Ratner , J. Chem. Phys. 93, 6484 (1990).

[14] F. Webster, P.J. Rossky, and R.A. Friesner, Comp. Phys. Comm. **63**, 493 (1991).

[15] R.N. Barnett, U. Landman and A. Nitzan, J. Chem Phys. 94, 608 (1991).

[16] E.J. Heller, J. Chem. Phys. **94**, 2723 (1991).

[17] K. Haug and H. Metiu, J. Chem. Phys. **95**, 5670 (1991).

[18] B. Hartke and E.A. Carter, Chem. Phys. Lett. 189, 358 (1992)

[19] M.J. Field, J. Chem. Phys. 96, 4583 (1992).

[20] E. Deumenes, A. Diz, H. Taylor and Y. Ohrn, J. Chem. Phys. 96, 6820 (1992).

[21] K. Haug and H. Metiu, J. Chem. Phys. **97**, 4781 (1992).

[22] J.B. Delos, W.R. Thorson and S.K. Knudson, Phys. Rev. A **6**, 709 (1972); J.B. Delos and W.R. Thorson Phys. Rev. A **6**, 720 (1972).

[23] H.D. Meyer and W. H. Miller, J. Chem. Phys. **70**, 3214 (1979).

[24] R. B. Gerber, V. Buch and M. A. Ratner, J. Chem. Phys. 77, 3022 (1982).

[25] D. Thirumalai, A.J. Bruskin and B.J. Berne, J. Chem. Phys. 83, 230 (1985).

[26] N. Makri and W.H. Miller, J. Chem. Phys. **87**, 5781 (1987).

[27] Z. Kotler, A. Nitzan, and R. Kosloff, Chem. Phys. Lett, **153**, 483 (1988).

[28] A. Garcia-Vela and R. B. Gerber, J. Chem. Phys. 98, 427 (1993).

[29] (a) E.J. Heller, J. Chem. Phys. **62**, 1544 (1975); **65**, 1289 (1976); **65**, 4979 (1976); **67**, 3339 (1977).

(b) S. Sawada, R. Heather, B. Jackson and H. Metiu, J. Chem. Phys. 83, 3009 (1985); R. Heather and H. Metiu, J. Chem. Phys. 84, 3250 (1986).

[30] V. Engel, R. Schinke, S. Hennig and H. Metiu, J. Chem. Phys. **92**, 1 (1990).

[31] E.J. Heller, J. Chem. Phys. **68**, 2066 (1978); **68**, 3891 (1978).

[32] (a) P.A.M. Dirac, Proc. Camb. Phil. Soc. 25, 62 (1929).

(b) A.D. McLachlan, Mol. Phys. 8, 39 (1964).

[33] J.A. Fleck, Jr., J.R. Morris and M.D. Feit, Appl. Phys. **10**, 129 (1976).

[34] M. Parrinello and A. Rahman, J. Chem. Phys. **80**,860 (1984).

[35] D.F. Coker, B.J. Berne and D. Thirumalai , J. Chem. Phys **86**, 5689 (1987).

[36] F.E. Budenholzer, E.A. Gislason, A.D. Jorgensen, J. Chem. Phys. **66**, 4832 (1977).

[37] (a) H.G. Kuhn, *Atomic Spectra* (Longmans, Green and Co. , 1969).
(b) A.R. Striganov and N.S. Sventitskii, *Tables of Spectral Lines of Neutral and Ionized Atoms*, (Plenum Press, New York, 1968).

[38] For an overall view, see: (a) D.W. Ball, Z.H. Kafafi, L. Fredin, R.H. Hauge and J.L. Margrave, editors, *A Bibliography of Matrix Isolation Spectroscopy 1954-1985* (Rice University Press, Houston, 1988).
The spectroscopy of alkali atoms in rare gas matrices can be found going back to :
(b) M. McCarty, Jr. and G.W. Robinson, Mol. Phys. **2**, 415 (1959); W. Weyhmann and F.M. Pipkin, Phys. Rev. **137**, A490 (1965); B. Meyer, J. Chem. Phys. **43**, 2986 (1965);
and a sample of more recent work includes :
(c) C. Samat, J.L. Rose, B.E. Williamson, and P.N. Schatz, Chem. Phys. Lett. **142**, 557 (1987) ;
(d) M.E. Fajardo, J. Chem. Phys. **98**, 110 (1993).

[39] F.A. Cotton and G. Wilkinson, *Advanced Inorganic Chemistry* , 4th ed. , p. 51, (John Wiley and Sons, New York, 1980).

[40] B. Hellsing, A. Nitzan and H. Metiu , Chem. Phys. Lett. **123**, 523 (1986).

[41] J. Schnitker, K.A. Motakabbir, P.J. Rossky and R. Friesner, Phys. Rev Lett. **60**, 456 (1988); K.A. Motakabbir and P.J. Rossky, Chem. Phys. 129, 253 (1989); K.A. Motakabbir, J. Schnitker and P.J. Rossky, J. Chem. Phys. 90, 6916 (1989).

[42] L. Verlet, Phys. Rev. **159**, 98 (1967).

TABLE I:

The oscillator strength (F_n) for the first three peaks in the spectrum is given in columns 2-4. The ionization potential (IP in eV) is given in column 5. The fundamental peak frequency (ω , in eV) in the spectrum is listed in column 6.

System	F_n in series n=1	n=2	n=3	IP (ev)	peak ω (eV)
K atom (expt.) [a]	0.968	0.009	0.001	4.34	1.61
K atom (calculated)	0.988	0.009	0.001	4.34	1.64
KXe_6 (calculated):					
Frozen Xe	0.962	0.027	0.008	4.77	1.97
QCT method	0.953	0.027	0.008	4.77	1.96
QCT method + $\eta(t)$	0.730	0.159	0.031	4.77	b
QGWP method	0.755	0.141	0.027	4.77	1.39

(a) Best fit to a variety of experimental and theoretical data.[37a]

(b) The peak frequency value for this case (7.94eV) is meaningless since energy shifts are being included via the Hartree phase term which are not being corrected for from the phase of the classical wave function.

FIGURE CAPTIONS

Fig. 1 The absorption spectrum (in arbitrary units) versus frequency (in eV) for the two-coordinate model problem using: (a) the time-dependent Hartree method ; (b) the QGWP approximation.

Fig. 2 The absorption spectrum (in arbitrary units) versus frequency (in eV) with the ⟨ 0,0,1 ⟩ polarization direction (along the K-Xe axis) for:
(a) the lone K atom ; (b) the frozen KXe_6 cluster ; (c) the KXe_6 cluster using the QCT approximation ; (d) the KXe_6 cluster using the QGWP approximation.

Fig. 3 The absorption spectrum (in arbitrary units) versus frequency (in eV) with the ⟨ 1,1,1 ⟩ polarization direction (between the K-Xe axes) for the KXe_6 cluster using the QGWP approximation. (a) The full spectrum on the 0-4 eV energy scale ; (b) the fundamental transition from part (a) showing the vibrational fine structure.

Fig. 4 For the KXe_6 cluster described in Fig. 3: (a) a representative coordinate R(t) , in Angstroms, giving the Xe-K distance for 4000fs ; (b) curve C is the energy of the classical degrees of freedom (in eV , on the left axis) and curve Q is the energy of the quantum degrees of freedom (in eV , on the right axis)

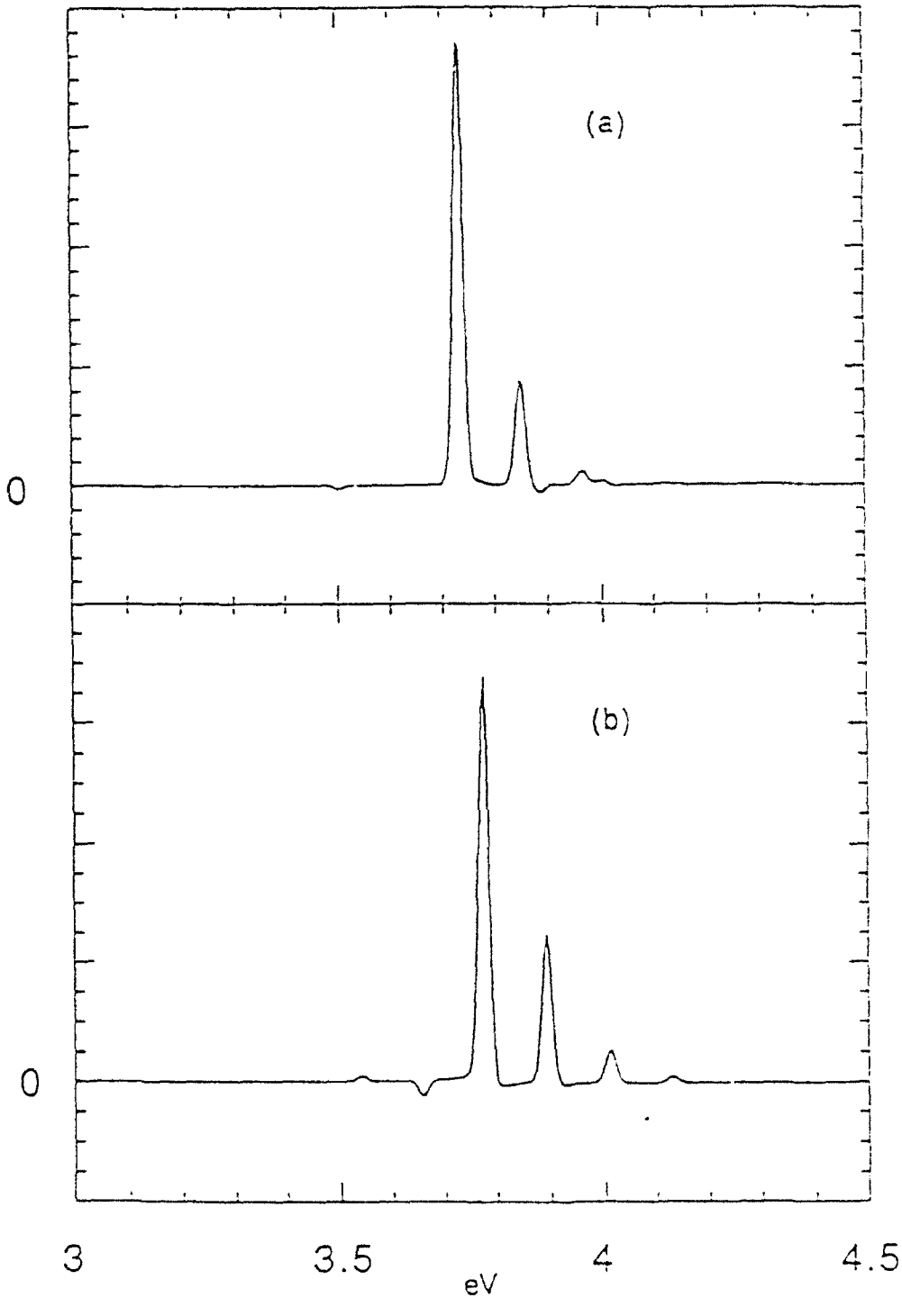

Fig. 1

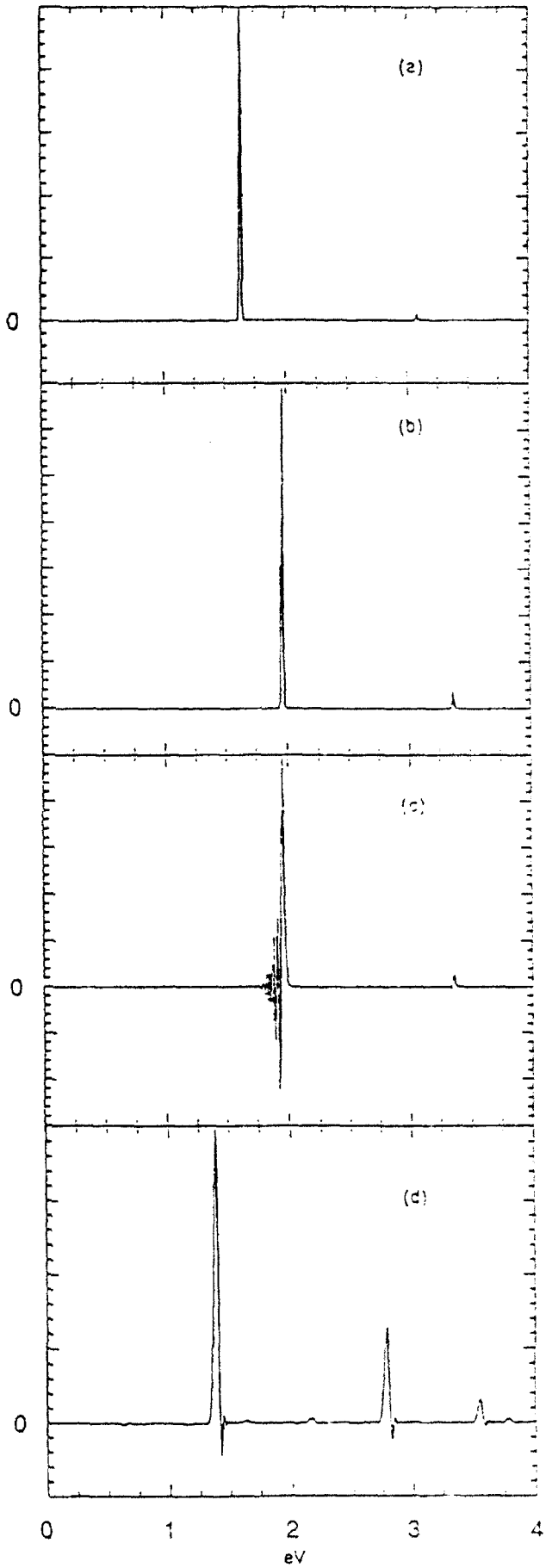

Fig 2

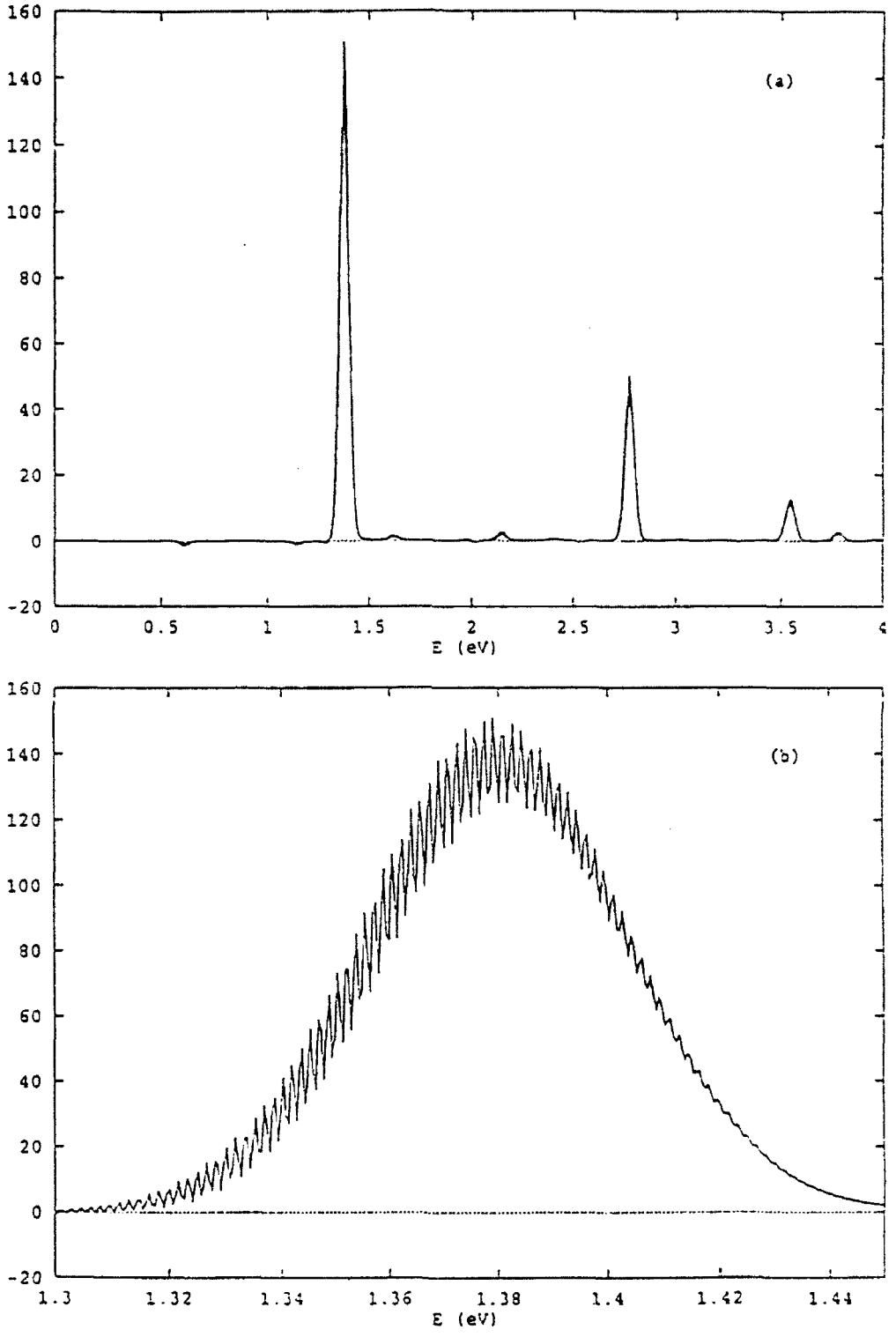
(a)
160
140
120
100
80
60
40
20
0
-20
0
0.5
1
1.5
2
2.5
3
3.5
E (eV)
(b)
160
140
120
100
80
60
40
20
0
-20
1.3
1.32
1.34
1.36
1.38
1.4
1.42
1.44
E (eV)

Fig. 3

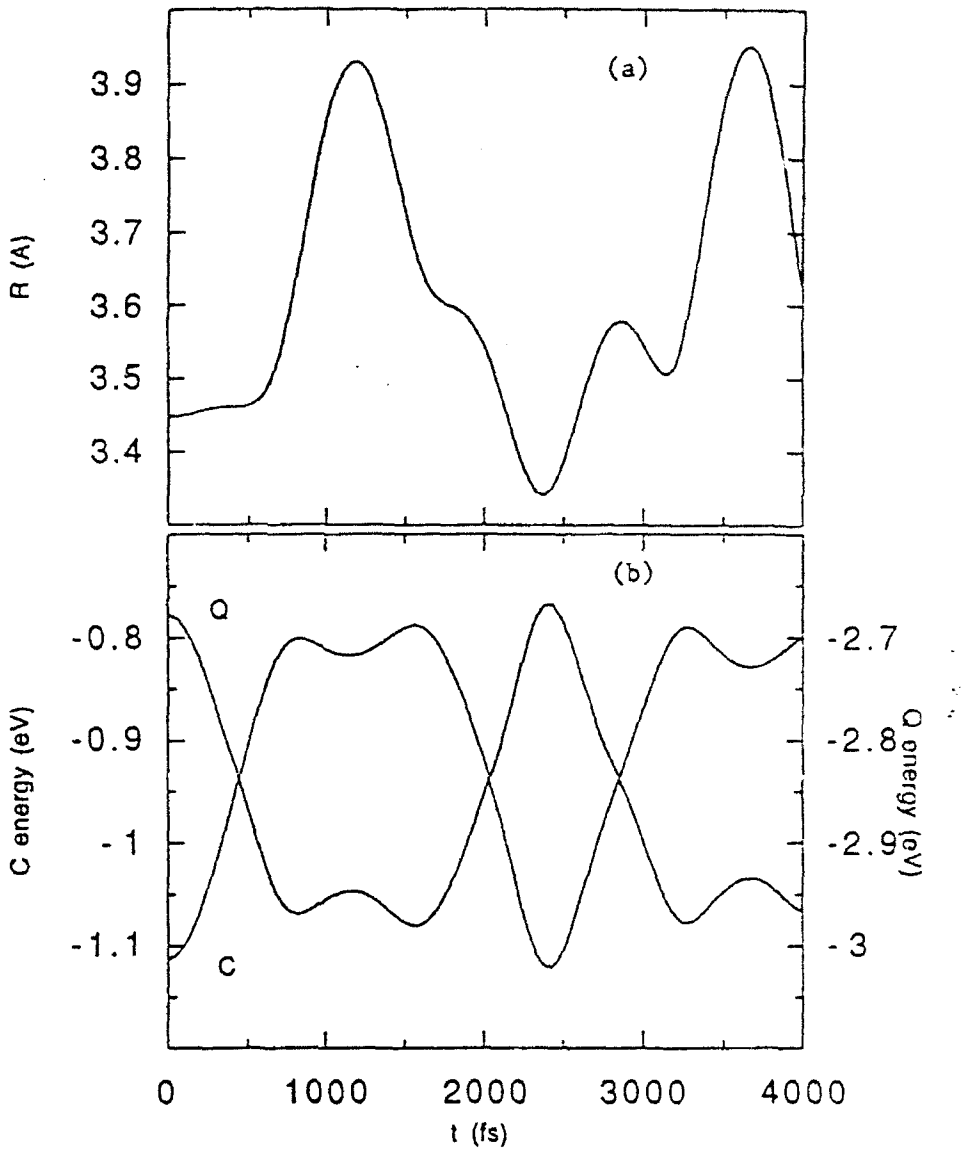
(a)
3.9
3.8
3.7
3.6
3.5
3.4
R (A)
(b)
Q
C
-0.8
-0.9
-1
-1.1
C energy (eV)
-2.7
-2.8
-2.9
-3
Q energy (eV)
0
1000
2000
3000
4000
t (fs)

Fig. 4

TECHNICAL REPORT DISTRIBUTION LIST - GENERAL

Office of Naval Research (2)*
Chemistry Division, Code 1113
800 North Quincy Street
Arlington, Virginia 22217-5000

Dr. James S. Murday (1)
Chemistry Division, Code 6100
Naval Research Laboratory
Washington, D.C. 20375-5000

Dr. Robert Green, Director (1)
Chemistry Division, Code 385
Naval Air Weapons Center
Weapons Division
China Lake, CA 93555-6001

Dr. Elek Lindner (1)
Naval Command, Control and Ocean
Surveillance Center
RDT&E Division
San Diego, CA 92152-5000

Dr. Bernard E. Douda (1)
Crane Division
Naval Surface Warfare Center
Crane, Indiana 47522-5000

Dr. Richard W. Drisko (1)
Naval Civil Engineering
Laboratory
Code L52
Port Hueneme, CA 93043

Dr. Harold H. Singerman (1)
Naval Surface Warfare Center
Carderock Division Detachment
Annapolis, MD 21402-1198

Dr. Eugene C. Fischer (1)
Code 2840
Naval Surface Warfare Center
Carderock Division Detachment
Annapolis, MD 21402-1198

Defense Technical Information
Center (2)
Building 5, Cameron Station
Alexandria, VA 22314

* Number of copies to forward